JOURNAL OF
EMERGING INVESTIGATORS

Article

Electrocatalytic oxidation of furfural on Co_3O_4/nickel foam catalyst: performance and mechanistic study

Qiumeng Song[1], Thomas J. Webster[2]
[1] Zhengzhou No.1&8, United International School, Zhengzhou, China
[2] Division of Pre-College and Undergraduate Studies, Brown University, Providence, RI, USA

SUMMARY

The electrocatalytic conversion of furfural into value-added chemicals, such as furoic acid, shows significant potential for sustainable chemical production. Furfural, derived from biomass, is a critical platform molecule for manufacturing biofuels, pharmaceuticals, and biodegradable plastics, making it economically and environmentally significant. However, understanding the catalyst's behavior during furfural oxidation remains challenging since furfural is high unstable and easily decomposes. In acidic environments often used for the catalysis of furfural, catalysts suffer from leaching and deactivation. The objective of the present study was to investigate cobalt oxide/nickel foam (Co_3O_4/NF) as a new catalyst due to its redox properties, high activity, and ability to easily transition between oxidation states, making it ideal for furfural electro-oxidation. We hypothesized that the unique redox properties of Co_3O_4, combined with the conductive nature of the NF substrate, would synergistically enhance catalytic performance for furfural oxidation. Our results showed that the Co_3O_4/NF composite had high activity and stability in furfural oxidation. Electrochemical tests revealed that the Co_3O_4/NF catalyst had a large electrochemical surface area, indicating a high number of active sites. Pulse tests showed that Co_3O_4 oxidized more easily than cobalt hydroxide carbonate ($Co_2(OH)_2CO_3$) or pristine nickel foam. As suggested, broken circuit process tests revealed that the Co^{3+} species that formed during electrocatalysis enhanced the spontaneous non-electrochemical oxidation rate of furfural. These results demonstrate the catalyst's high activity and selectivity, offering insights into the design of efficient, stable electrocatalysts for biomass-derived chemicals. This study also advanced an understanding of surface dynamics in transition metal oxides during electrocatalysis, paving the way for the next generation of catalysts.

INTRODUCTION

The increasing demand for sustainable energy solutions has led to the exploration of renewable energy sources (such as wind, solar, hydropower, and biomass) to drive critical chemical processes, like water splitting for hydrogen (H_2) production (1–6). These approaches strive to find alternatives to mitigate the environmental and energy challenges posed by the continued reliance on fossil fuels (7). The transition from fossil fuels to renewable energy is essential to reduce the environmental challenges posed by greenhouse gas emissions and climate change. Biomass, including agricultural waste, has emerged as a promising resource due to its abundance, renewability, and potential to produce chemicals of value to energy, biofuels, medicine, and/or other applications important to society (8). Furfural, a biomass-derived compound, has gained attention as a renewable feedstock for the production of value-added chemicals such as furoic acid, which can be used in the synthesis of biodegradable polymers and pharmaceuticals (9–11). Typical furoic acid selectivity in electrocatalytic systems ranges from 60–80%, depending on the catalyst and reaction conditions, making it a key benchmark for evaluating catalytic performance (12).

However, one of the key obstacles in the process of producing furoic acid from furfural is the slow kinetics of the anodic oxygen evolution reaction, which involves a complex four-electron transfer, resulting in high energy consumption (13). Furfural oxidation also remains challenging since furfural is highly unstable and easily decomposes (13). In acidic environments often used for the catalysis of furfural, catalysts suffer from leaching and deactivation (13). An effective strategy to reduce energy consumption is to replace the oxygen evolution reaction with alternative nucleophilic oxidation reactions, such as the oxidation of hydroxyl groups and aldehydes, which can simultaneously produce value-added chemicals (14). The choice of electrocatalyst plays a critical role in these reactions, as different catalysts can alter the reaction pathway, kinetics, and overall energy efficiency. Among transition metal-based electrocatalysts, cobalt-based materials have shown significant potential for nucleophilic oxidation reactions (15). Notably, nucleophilic oxidation reactions have been found to be closely linked to the Co^{2+}/Co^{3+} redox reactions, yet the redox kinetics of these species and their direct impact on electrocatalytic performance remain under-explored (16).

In this study, we hypothesized that the unique redox properties of cobalt oxide (Co_3O_4), combined with the conductive nature of the nickel foam (NF) substrate, would synergistically enhance the catalytic performance for furfural oxidation (17–18). Nickel foam was chosen as the substrate due to its high conductivity, large surface area, and mechanical stability, which have been shown to enhance the performance of electrocatalysts in previous studies (19–27). Here, we successfully synthesized Co_3O_4 nanoflowers directly grown on NF and tested their capacity to serve as a highly efficient electrocatalyst for furfural oxidation.

The Co_3O_4/NF composite demonstrated excellent catalytic performance for furfural oxidation, showing significantly higher activity than its precursor materials. Comparative studies revealed that the unique structure of Co_3O_4 facilitates more efficient redox processes, leading

https://doi.org/10.59720/24-333

to improved reaction kinetics. These findings underscore the capability of Co_3O_4/NF as a superior electrocatalyst for furfural oxidation, highlighting its potential for applications in biomass-derived chemical transformations and sustainable catalytic processes. Beyond furfural oxidation, this study offers broader implications for sustainable chemistry by establishing design principles for efficient nucleophilic oxidation reaction catalysts, demonstrating an energy-saving alternative to conventional oxygen evolution reaction-coupled processes, and showcasing how biomass conversion can be integrated with renewable energy systems.

RESULTS

Synthesis and characterization of Co_3O_4/NF

In this study, we successfully employed Co_3O_4/NF as a model catalyst to investigate its catalytic performance in furfural oxidation, providing valuable insights into the underlying mechanisms driving its high activity. The Co_3O_4/NF synthesis process diagram provides an overview of the in situ growth and transformation steps **(Figure 1a)**. Briefly, for this, a piece of pre-cleaned NF was fully submerged in a solution of cobalt nitrate hexahydrate and urea dissolved in deionized water and was stirred continuously. After a hydrothermal reaction and cleaning, the $Co_2(OH)_2CO_3$/NF was dried under a vacuum at 60°C for 6 hours to form $Co_2(OH)_2CO_3$ nanoflowers on the NF substrate. The $Co_2(OH)_2CO_3$/NF material was placed in a muffle furnace and subjected to heat treatment at 350°C for two hours in an air atmosphere to form Co_3O_4/NF nanoflowers.

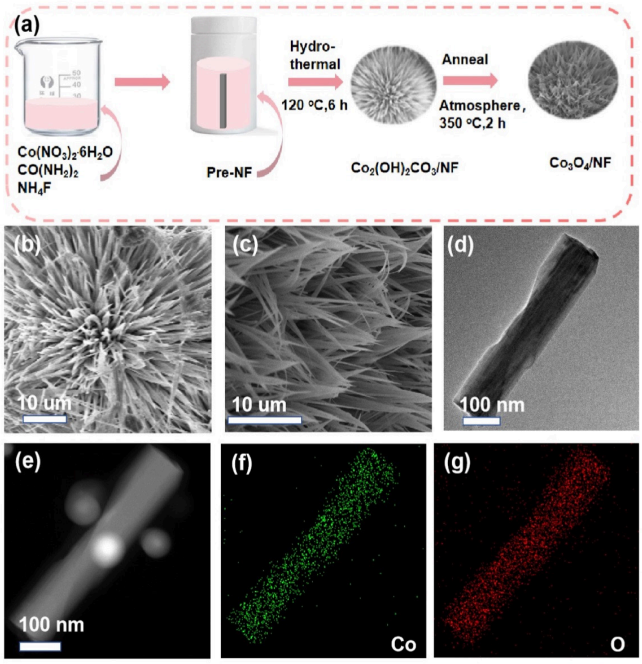

Figure 1. Synthesis and characterization of $Co_2(OH)_2CO_3$/NF and Co_3O_4/NF. (a) Schematic diagram of the catalyst's synthesis process; (b) scanning electron microscope (SEM) image of $Co_2(OH)_2CO_3$/NF showing its nano-petal structure; (c) SEM image of Co_3O_4/NF, demonstrating the retained nano-petal morphology after oxidation; (d) transmission electron microscope (TEM) image of Co_3O_4/NF providing detailed structural insight; and (e) scanning tunnel electron microscope (STEM) image of Co_3O_4/NF and corresponding elemental mappings of (f) cobalt (Co) and (g) oxygen (O).

In terms of material characterization, scanning electron microscopy (SEM) imaging of $Co_2(OH)_2CO_3$ revealed a distinctive nano-petal-like structure, characterized by thin, petal-shaped formations **(Figure 1b)**. Similarly, the SEM image of Co_3O_4 confirmed that the nanostructure remained largely intact after the thermal oxidation of $Co_2(OH)_2CO_3$ in air, preserving the nano-petal morphology **(Figure 1c)**. Transmission electron microscopy (TEM) imaging of Co_3O_4, further corroborated the nano-petal structure at higher resolution, emphasizing its structural consistency post-calcination **(Figure 1d)**. Dark-field imaging, along with element mapping, provided critical insights into the elemental distribution **(Figure 1e-g)**. Element mapping demonstrated that cobalt (Co) and oxygen (O) were uniformly distributed across the nanopetals, confirming the homogeneity of the Co_3O_4 nanoflowers. This even dispersion of elements is a key factor contributing to the material's high catalytic performance, as it ensures the availability of active sites throughout the structure (28). These characterizations collectively highlight the stability and uniformity of the synthesized Co_3O_4/NF catalyst, which is crucial for its enhanced electrochemical activity in catalysis.

Electrocatalytic performance of Co_3O_4/NF for furfural oxidation

The electrocatalytic performance of the samples for furfural oxidation was evaluated using linear sweep voltammetry under a three-electrode system. Our electrochemical analysis revealed that Co_3O_4 exhibited high selectivity (~80%) for furoic acid production, with the remaining products consisting primarily of furfuryl alcohol (10%) and trace amounts of 5-hydroxymethylfurfural and other oligomeric side products (10%), and a Faradaic efficiency of approximately 90% under alkaline conditions, demonstrating its potential for sustainable chemical synthesis **(Figure 2)**. Co_3O_4/NF demonstrated superior catalytic activity for both the oxygen evolution reaction and furfural oxidation reaction compared to $Co_2(OH)_2CO_3$/NF and pristine nickel foam (Pre-NF) **(Figure 2a)**. Notably, the onset potential of Co_3O_4 was lower than that of $Co_2(OH)_2CO_3$ and Pre-NF, indicating enhanced electrocatalytic efficiency. This lower onset potential suggests that Co_3O_4/NF requires less energy to initiate the oxidation process, contributing to its catalytic performance.

Chronoamperometry tests, conducted after 30 minutes of furfural oxidation reaction, revealed that Co_3O_4/NF exhibited a higher furoic acid yield compared to $Co_2(OH)_2CO_3$/NF and Pre-NF **(Figure 2b)**. Interestingly, the furoic acid yield increased with applied potential between 1.40 VRHE and 1.60 VRHE, with Co_3O_4/NF reaching its maximum yield at 1.6 VRHE. While the upward trend suggests that further increases in potential might enhance furoic acid production, stability considerations and possible catalyst degradation at higher potentials limited our testing range.

Furthermore, the furoic acid production rate of Co_3O_4/NF surpassed that of the other catalysts **(Figure 2c)**. Additionally, the system achieved over 90% Faradaic efficiency and 80% furoic acid yield within the tested potential range, demonstrating the good performance of Co_3O_4/NF in furfural oxidation **(Figure 2d)**.

https://doi.org/10.59720/24-333

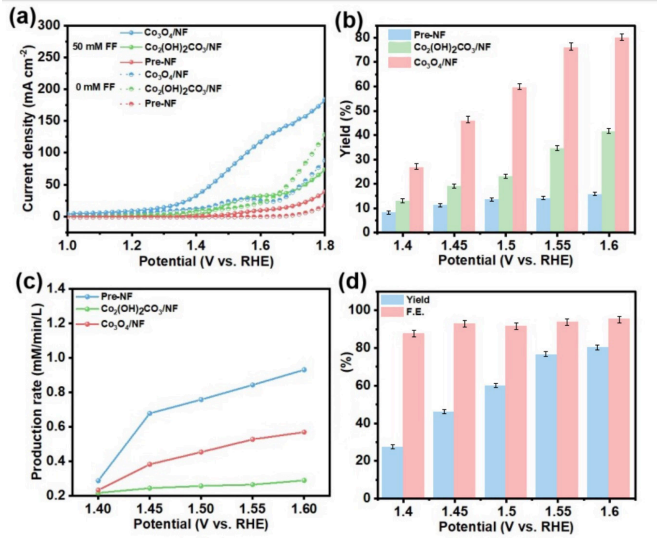

Figure 2. Furfural oxidation reaction performance in a three-electrode system. (a) LSV curves of the three catalysts at a scan rate of 5 mV s^{-1} in 1.0 M KOH with and without 50 mM furfural; (b) Furoic acid yield comparison for different catalysts; (c) Furoic acid production rate after 30 minutes of the furfural oxidation reaction process; and (d) Faradaic efficiency (FE) and furoic acid yield of furfural oxidation over the Co_3O_4/NF catalyst after 30 minutes of furfural oxidation reaction. Experiments were conducted in triplicate (n = 3).

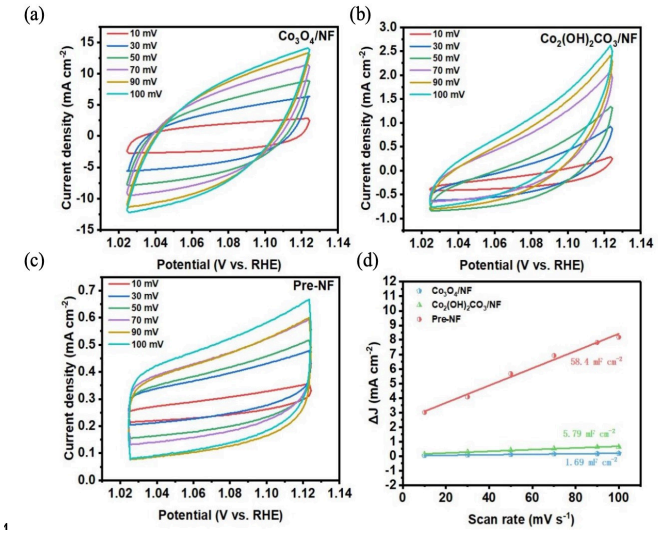

Figure 3. Cyclic voltammetry (CV) curves of furfural conversion. (a) Co_3O_4/NF, (b) $Co_2(OH)_2CO_3$/NF and (c) Pre-NF catalysts in the non-faradaic region, measured at scan rates of 10, 30, 50, 70, 90, and 100 mV/s. (d) Corresponding double-layer capacitance (Cdl) measurements at 1.07 V for all three catalysts, reflecting their electrochemical surface areas (ANOVA, $p = 0.01$ for (a) compared to (b) and (c) and $p = 0.045$ for (b) compared to (c)).

Electrochemical active surface area and active sites

The electrochemical active surface area (ECSA) is a critical parameter in electrocatalysis as it directly correlates with the number of available active sites for reactions. The ECSA of the catalysts was determined using cyclic voltammetry in the non-faradaic region, where the double-layer capacitance was measured at various scan rates. The ECSA was then calculated from the slope of the capacitive current versus scan rate plot. The Co_3O_4/NF nanoflowers displayed an impressive ECSA of 58 mF/cm², confirming the high density of catalytic sites available for reaction **(Figure 3)**. Further, the ECSA of Co_3O_4/NF (58.4 ± 2.1 mF/cm²) is notably larger than that of $Co_2(OH)_2CO_3$/NF (5.79 ± 0.3 mF/cm²) and Pre-NF (1.69 ± 0.1 mF/cm²) (ANOVA, $p = 0.02$) **(Figure 3)**. This increase in active area correlates with the enhanced catalytic performance of Co_3O_4/NF, confirming its superior activity in both furfural oxidation reaction and oxygen evolution reaction compared to $Co_2(OH)_2CO_3$/NF and Pre-NF **(Figure 3a)**. The larger ECSA suggests a greater density of active sites on Co_3O_4/NF, contributing to its heightened catalytic efficiency in these reactions.

Deprotonation ability and redox properties

Deprotonation is a critical step in electrocatalytic reactions, particularly in the furfural oxidation reaction. During these processes, the removal of protons (H^+) from intermediate species, such as Co(II)-OH or Co(III)-OOH, facilitates the formation of active oxygen species and enhances the overall catalytic activity. The ability of a catalyst to undergo deprotonation efficiently is often linked to its redox properties and the ease with which it can transition between oxidation states. In this study, the deprotonation ability of the catalysts was evaluated by measuring the charge accumulation rate on the catalyst surface under periodic pulse voltages, which reflects the rate at which protons are removed during the reaction.

During the oxidation of the catalyst in the oxygen evolution reaction process, pulsed voltammetry tests were conducted to further assess the deprotonation ability of the catalysts **(Figure 4)**. During the oxygen evolution reaction process of the Co_3O_4 catalyst in the alkaline solution, $Co_2(OH)_2CO_3$ forms on the surface and subsequently deprotonates to generate Co(III)-OOH species. The deprotonation ability of the catalyst can be evaluated by measuring the charge accumulation rate on the surface under periodic pulse voltages. Pulse tests showed that Co_3O_4 undergoes oxidation more readily than its counterparts, $Co_2(OH)_2CO_3$ and Pre-NF **(Figure 4)**. Co_3O_4's deprotonation capacity was significantly higher than that of $Co_2(OH)_2CO_3$ ($t(4) = 5.32$, $p = 0.003$) and Pre-NF ($t(4) = 8.47$, $p < 0.001$), further enhancing Co_3O_4's electrocatalytic activity **(Figure 4)**. To ensure comparability, all electrochemical data were normalized to ECSA. The relationship between the total accumulated oxide charge density (QECSA) and the pulse voltage (high potential Eh) showed a linear trend **(Figure 4b)**. The slope of this relationship reflects the deprotonation ability of the catalyst. The slope values for Co_3O_4, $Co_2(OH)_2CO_3$, and Pre-NF are 0.154, 0.145, and 0.065, respectively, indicating the deprotonation capacity follows the order: Co_3O_4 > $Co_2(OH)_2CO_3$ > Pre-NF **(Figure 4b)**. In addition, the deprotonation ability of these catalysts is inversely related to their onset potential **(Figure 4c)**. A stronger deprotonation capacity correlates with a lower onset potential, making it easier for Co^{2+} to oxidize, thus enhancing the catalytic activity for the furfural oxidation reaction and oxygen evolution reaction processes.

https://doi.org/10.59720/24-333

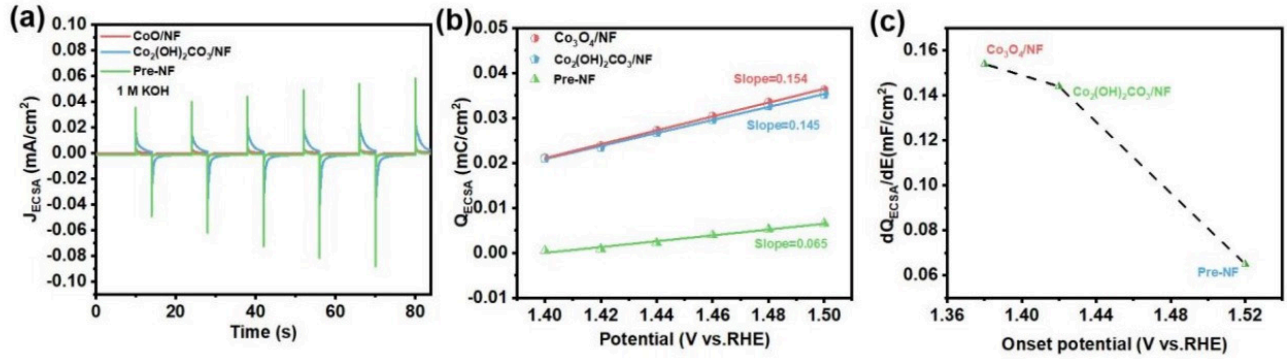

Figure 4. Pulsed voltammetry analysis of catalyst deprotonation kinetics. (a) Pulse voltammetry protocol applied between 1.15 V vs. RHE (low potential) and 1.4 V to 1.5 V vs. RHE (high potential), without iR correction. (b) Charge density (QECSA) versus pulse voltage for different catalysts, derived from pulse-voltammetry tests. (c) The correlation between the onset potential and the deprotonation ability of the catalysts, highlighting the impact of proton removal on catalytic efficiency.

Spontaneous non-electrochemical reactions and kinetics

To investigate the effect of spontaneous non-electrochemical reactions on furfural oxidation reaction activity, broken circuit process (BCP) tests were employed to analyze differences in spontaneous chemical reaction kinetics. During the standard BCP process in the 1 M potassium hydroxide (KOH) solution (BCP-KOH), all catalysts showed a discharge curve at low potential due to surface charge accumulation at high potential, forming Co(III)-OOH. The discharge magnitude followed the order: Co_3O_4 > $Co_2(OH)_2CO_3$ > Pre-NF, indicating greater surface charge accumulation of Co(III)-OOH in Co_3O_4. However, when the optimized BCP process was conducted in 1 M KOH with 50 mM furfural (BCP-FF), the discharge curve disappeared, suggesting a spontaneous non-electrochemical reaction between Co(III)-OOH and furfural during the furfural oxidation reaction process.

The results from both the standard (BCP-KOH) and optimized (BCP-FF) BCP tests provided critical evidence that Co_3O_4 facilitates the spontaneous oxidation of furfural at a significantly faster rate than $Co_2(OH)_2CO_3$ and Pre-NF, emphasizing the superior kinetics of Co_3O_4 in the reaction process **(Figure 5)**. To quantitatively assess the kinetics of these spontaneous reactions, an optimized BCP-KOH-FF process was designed **(Figure 5g)**. The test involved BCP i-t measurements as explained in the methods section. By varying the BCP duration, Q_t-t curves were obtained, revealing the spontaneous reaction rates: Co_3O_4 > $Co_2(OH)_2CO_3$> Pre-NF **(Figure 5h)**. Using the first-order kinetic equation $\ln(Q_0/Q_t) = kt$, where k is the rate constant, the linear fitting results confirmed the order of reaction kinetics: Co_3O_4 > $Co_2(OH)_2CO_3$ > Pre-NF **(Figure 5i)**.

DISCUSSION

As hypothesized, the Co_3O_4/NF composite exhibited outstanding catalytic performance, achieving an impressive 80% selectivity towards furoic acid and a high Faradaic efficiency of 90% under optimal conditions. Detailed electrochemical analysis revealed that the Co_3O_4/NF catalyst possessed an ESCA of 58.4 mF/cm^2, indicating an enormous density of active catalytic sites. Furthermore, pulse testing demonstrated that Co_3O_4 undergoes oxidation more readily than cobalt hydroxide carbonate ($Co_2(OH)_2CO_3$) and pristine NF, suggesting its enhanced redox properties. The optimized BCP tests further confirmed that the formation of the Co^{3+} species in Co_3O_4 accelerates the spontaneous oxidation of furfural, offering an improvement in reaction kinetics over $Co_2(OH)_2CO_3$ and bare NF. These findings not only highlight the superior catalytic performance of Co_3O_4 but also offer a clearer understanding of how its intrinsic properties, such as redox flexibility and surface dynamics, contribute to enhanced reactivity. The redox flexibility of Co_3O_4, particularly the facile Co^{2+}/Co^{3+} transition observed in our pulse voltammetry studies, suggests this material could be further tuned for other value-added chemical syntheses beyond furfural oxidation. Our results specifically indicate that engineering metal oxides with nanoflower morphologies and optimized hydroxylation/deprotonation characteristics may unlock new opportunities in sustainable electrosynthesis – potentially replacing traditional precious-metal catalysts in biorefinery applications.

One limitation of this study is the absence of in situ spectroscopic techniques to monitor the oxidation states of Co_3O_4 during the electrocatalytic reactions. While the pulse and BCP tests provided valuable insights into the redox behavior and reaction kinetics, they do not offer direct evidence of the formation and role of intermediate species, such as Co(III)-OOH, during the oxidation process. This limits our understanding of the detailed reaction mechanism.

In addition, the experiments were conducted under a specific set of conditions (e.g., alkaline medium and fixed concentration of furfural). While these conditions were optimized for high selectivity and Faradaic efficiency, they may not fully represent the performance of Co_3O_4/NF under varying pH levels, temperatures, or reactant concentrations. Exploring a broader range of conditions could provide a more comprehensive understanding of the catalyst's performance. Further mechanistic studies could be carried out using in situ spectroscopic techniques. For example, X-ray absorption near-edge structure (XANES) could provide element-specific information about the oxidation state and local coordination environment of cobalt centers, helping to track redox transitions between Co^{2+} and Co^{3+} during the reaction. Additionally, infrared spectroscopy could detect surface-

https://doi.org/10.59720/24-333

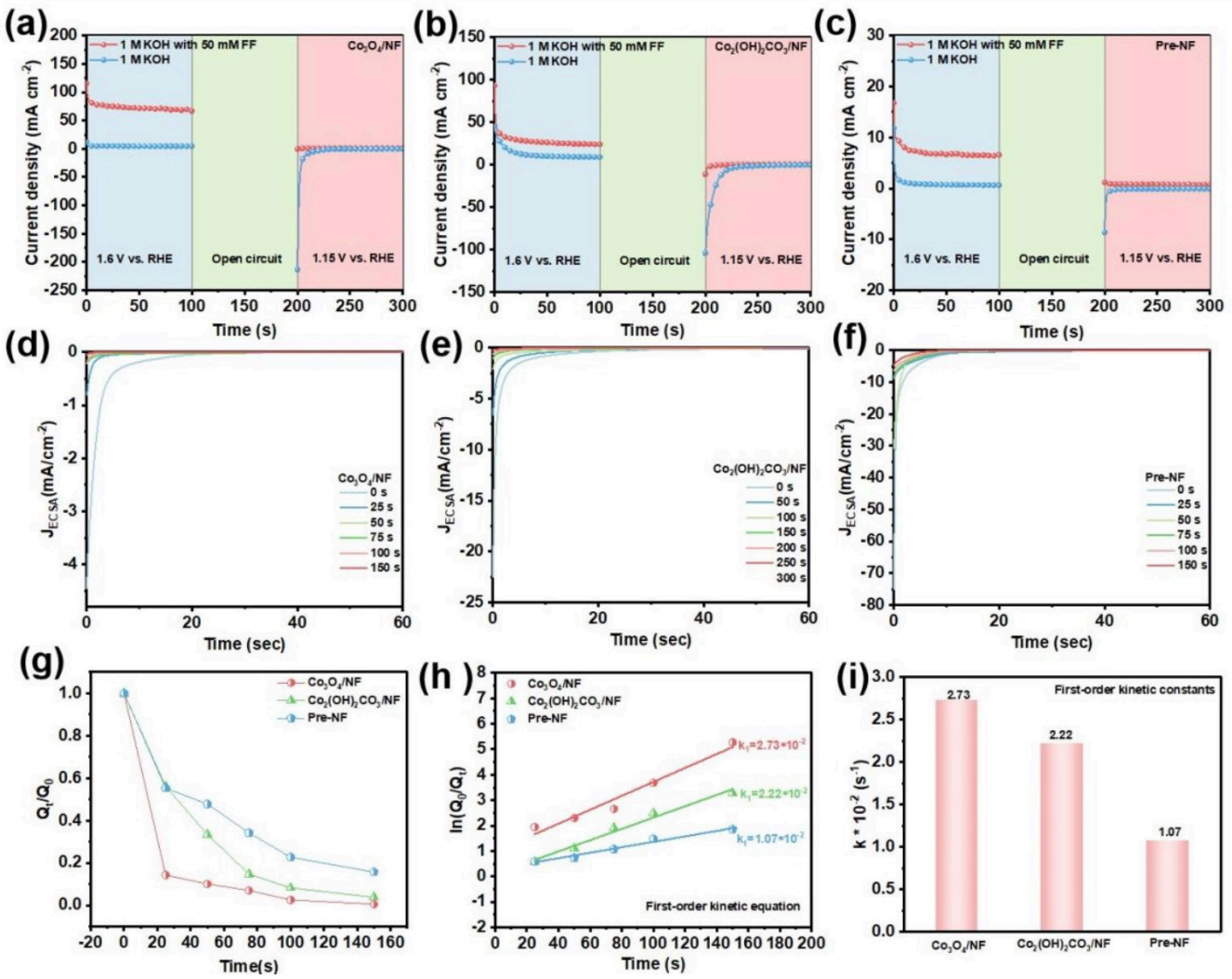

Figure 5. Analyzing differences in spontaneous reaction kinetics through bi-segment amperometric (BCP) tests. (a-c) The BCP test results for Co_3O_4, $Co_2(OH)_2CO_3$ and Pre-NF, respectively. (d), (e), and (f) display the multi-potential step measurements for Co_3O_4, $Co_2(OH)_2CO_3$ and Pre-NF in a 1.0 M KOH solution, both with and without the presence of 50 mM furfural. (g) The plots of Q_t/Q_0 versus time (t), derived from the optimized BCP-KOH-furfural tests, (h) the corresponding linear fitting of kinetic constants using a first-order kinetics equation for Co_3O_4, $Co_2(OH)_2CO_3$ and Pre-NF catalysts, and (i) rate constants for Co_3O_4, $Co_2(OH)_2CO_3$ and Pre-NF catalysts. Experiments were conducted in triplicate (n = 3).

adsorbed intermediates formed during furfural oxidation, offering insights into the reaction pathway. They could be employed during the electrocatalytic reactions to monitor the oxidation states of Co_3O_4. This would provide deeper insights into the reaction mechanism, particularly the formation and role of intermediate species (such as Co(III)-OOH) during the oxidation process.

Moreover, creating intentional distortions in the crystal structure of Co_3O_4 to influence d-orbital splitting and improve its catalytic performance is another intriguing experimental direction. Distortion in the crystal lattice can lead to the formation of the dx^2-y^2 orbital with a higher energy level. This means the dx^2-y^2 orbital will be closer to the Fermi level and hence the catalyst will have a stronger deprotonation ability. We can achieve this by either cation doping or creating oxygen vacancies in the Co_3O_4 lattice. To validate these modifications, X-ray diffraction would reveal changes in crystal symmetry by tracking diffraction pattern shifts, while X-ray photoelectron spectroscopy could quantify alterations in cobalt's oxidation states and oxygen vacancy concentrations via binding energy analysis.

Overall, our study highlights the promising future Co_3O_4 has for advanced electrocatalysts in biomass-derived chemical transformations and improved alternative energy applications. This technology could play a significant role in reducing reliance on fossil fuels by providing a renewable pathway for producing industrial chemicals and fuels. Furthermore, the integration of electrocatalytic processes with renewable energy sources, such as solar or wind power, could enable carbon-neutral chemical production, aligning with global efforts to combat climate change. In a broader scientific context, this work contributes to the growing body of research on transition metal oxides and their applications in electrocatalysis, paving the way for the development of

https://doi.org/10.59720/24-333

next-generation catalysts with enhanced performance and stability.

MATERIALS AND METHODS

Chemicals and reagents

The chemicals used included hydrochloric acid (HCl) (Sigma-Aldrich), ethanol (C_2H_5OH) (Fisher Scientific), cobalt nitrate hexahydrate ($Co(NO_3)_2 \cdot 6H_2O$) (Sigma-Aldrich), urea ($CO(NH_2)_2$) (Alfa Aesar), ammonium fluoride (NH_4F) (Sigma-Aldrich), KOH (Sigma-Aldrich), furfural (Alfa Aesar), furoic acid (Sigma-Aldrich), NF (MTI Corporation), and deionized water.

Preparation of $Co_2(OH)_2CO_3$/NF

NF underwent precleaning through ultrasonic cleaning for 10 minutes each with ethanol, 3 M HCl, and deionized water to ensure its surface was free from contaminants.

For the synthesis of $Co_2(OH)_2CO_3$ nanoflowers, 3 mmol cobalt nitrate hexahydrate and 9 mmol urea were dissolved in 30 mL of deionized water. This solution was stirred continuously for 30 minutes to ensure homogeneity. Next, a piece of pre-cleaned NF was fully submerged in the solution and heated to 180°C for 12 hours.

After the hydrothermal reaction, the $Co_2(OH)_2CO_3$/NF product was thoroughly rinsed with both deionized water and ethanol to remove any residual reactants. Finally, the cleaned material was dried under vacuum at 60°C for 6 hours to complete the synthesis. This method resulted in the successful growth of $Co_2(OH)_2CO_3$ nanoflowers on the nickel foam substrate.

Preparation of Co_3O_4/NF

For the synthesis of Co_3O_4 nanoflowers, the process involved a calcination process of the pre-synthesized $Co_2(OH)_2CO_3$/NF. The $Co_2(OH)_2CO_3$/NF material was placed in a muffle furnace and subjected to heat treatment at 350°C for two hours in an air atmosphere. This controlled calcination process facilitated the oxidation of cobalt hydroxide carbonate ($Co_2(OH)_2CO_3$/NF) into cobalt oxide (Co_3O_4). The elevated temperature in the air not only ensured complete conversion but also maintained the structural integrity of the nanoflowers during the transformation. This procedure resulted in the formation of Co_3O_4 nanoflowers anchored onto the NF.

Material characterization

Samples were imaged using a JSM-7500F JEOL SEM (5kV) which shows the morphology of the catalyst. An EM-2011 TEM with an accelerating voltage of 200kV was used to observe the particle size of the nanoparticles.

Electrochemical furfural oxidation reaction performance testing

The catalyst synthesized in each experimental section was cut into a size of 1.0 cm × 1.5 cm and clamped with a platinum electrode clip, ensuring a contact area of 1.0 cm² with the electrolyte. This served as the working electrode, directly used for electrochemical testing.

All electrochemical tests were conducted in an H-type electrolytic cell separated by a Nafion 117 proton membrane, using a CHI660E electrochemical workstation (Shanghai Chenhua). In this study, all voltages were converted to the potential relative to the reversible hydrogen electrode (RHE) based on the Nernst equation:

$$E(vs.RHE) = E(vs.Ag/AgCl) + 0.059 \times pH + 0.197 \quad \text{...(Equation 1)}$$

where E (vs. RHE) represents the potential relative to the reversible hydrogen electrode, and EEE (vs. Ag/AgCl) is the electrode potential measured relative to the saturated Ag/AgCl reference electrode.

A standard three-electrode system was used to measure the electrocatalytic furfural oxidation reaction and oxygen evolution reaction performance of the catalyst. The reference electrode was a saturated Ag/AgCl, the counter electrode was a graphite rod and the working electrode was the prepared catalyst. The electrolyte was a 1.0 M KOH solution containing 50 mM furfural (or without furfural). The testing conditions for linear sweep voltammetry were a voltage range of 0–0.8 V vs. Ag/AgCl and a scan rate of 5 mVs^{-1}. The conditions for testing the ECSA were a voltage range of 0.0–100 mV vs. Ag/AgCl and scan rates of 10, 30, 50, 70, 90 and 100 mVs^{-1}. The conditions for electrochemical impedance spectroscopy (EIS) were an AC voltage amplitude of 5 mV, a frequency range of 0.01–105 Hz and the potential corresponding to a current density of 10 mA/cm^2.

For the BCP tests, the charging process lasted 100 s under a high potential of 1.60 V vs. RHE in a 1 M KOH solution. This was followed by a BCP process in a 1 M KOH^+ 50 mM furfural solution and a final discharge at a low potential of 1.15 V vs. RHE for 60 s. The discharge i-t curve reflected the reduction of Co(III)-OOH, and the discharge quantity (Q_t) was calculated by integrating the discharge current.

Statistical tests

Each experiment was conducted in triplicate, and the results are represented as mean ± standard deviation. Differences between means were determined using ANOVA followed by Tukey's HSD post-hoc tests and/or Student's t-tests. Graphs were generated using Excel.

ACKNOWLEDGMENTS

This work was funded by the Henan Institute of Advanced Technology, Zhengzhou University. We would like to express our greatest thanks to the lab supervisor Prof. Jingmin Ge and the lab instructor Prof. Zhikun Peng for their guidance with the safety requirements during operation, as well as for providing us with advice and encouragement throughout the project.

Received: November 01, 2024
Accepted: May 20, 2025
Published: July 19, 2026

REFERENCES

1. Alothman, A. A., et al. "Facile Fabrication of $CuScS_2$/CoO as an Efficient Electrocatalyst for Oxygen Evolution Reaction and Water Treatment Process." International *Journal of Hydrogen Energy*, vol. 49, 2024, pp. 564-579. https://doi.org/10.1016/j.ijhydene.2023.08.215.

https://doi.org/10.59720/24-333

2. Dang, Y., et al. "Hierarchical CoO@MoN Heterostructure Nanowire Array as a Highly Efficient Electrocatalyst for Hydrogen Evolution." *Chemical Engineering Journal*, Vol. 477, 2023. https://doi.org/10.1016/j.cej.2023.147154.
3. Diao, L., et al. "NaCl Sealing Strategy-Assisted Synthesis CoO-Co Heterojunctions as Efficient Oxygen Electrocatalysts for Zn Air Batteries." *Journal of Colloid and Interface Science*, vol. 645, 2023, pp. 329-337. https://doi.org/10.1016/j.jcis.2023.04.080.
4. Du, T., et al. "CoO/NiFe LDH Heterojunction as a Photo-Assisted Electrocatalyst for Efficient Oxygen Evolution Reaction." *International Journal of Hydrogen Energy*, vol. 51, 2024, pp. 907-915. https://doi.org/10.1016/j.ijhydene.2023.09.040.
5. Guo, J.-X., et al. "High Electrocatalytic Hydrogen Evolution Activity on a Coupled Ru and CoO Hybrid Electrocatalyst." *Journal of Energy Chemistry*, vol. 37, 2019, pp. 143-147. https://doi.org/10.1016/j.jechem.2018.12.011.
6. Ran, J., et al. "Co@CoO Chiral Nanostructures Enabling Efficient Oxygen Electrocatalysis by Modulated Spin-Polarization." *Chemical Engineering Journal*, vol. 493, 2024. https://doi.org/10.1016/j.cej.2024.152545.
7. Ren, X., et al. "Porous CoO-CeO_2 Heterostructures as Highly Active and Stable Electrocatalysts for Water Oxidation." *International Journal of Hydrogen Energy,* vol. 43, no. 50, 2018, pp. 22529–22537. https://doi.org/10.1016/j.ijhydene.2018.10.096.
8. Wang, C., et al. "Active Co@CoO Core/Shell Nanowire Arrays as Efficient Electrocatalysts for Hydrogen Evolution Reaction." *Chemical Engineering Journal*, vol. 429, 2022. https://doi.org/10.1016/j.cej.2021.132226.
9. Zhang, H., et al. "Interfacial FeOOH/CoO Nanowires Array Improves Electrocatalytic Water Splitting." *Journal of Solid State Chemistry*, vol. 298, 2021. https://doi.org/10.1016/j.jssc.2021.122156.
10. Zhang, K., et al. "N-Doped CoO Nanowire Arrays as Efficient Electrocatalysts for Oxygen Evolution Reaction." *Journal of Energy Chemistry*, vol. 37, 2019, pp. 13-17. https://doi.org/10.1016/j.jechem.2018.11.013.
11. Chen, S., et al. "Electrocatalytic Nitrate-to-Ammonia Conversion on CoO/CuO Nanoarrays Using Zn–Nitrate Batteries." *Nanoscale*, vol. 15, no. 48, 2023, pp. 19577-19585. https://doi.org/10.1039/d3nr05254k.
12. Chu, K., et al. "Efficient Electrocatalytic N_2 Reduction on CoO Quantum Dots." *Journal of Materials Chemistry A,* vol. 7, no. 9, 2019, pp. 4389-4394. https://doi.org/10.1039/c9ta00016j.
13. Gan, J., et al. "Platelet Carbon Nanofibers as Support of Pt-CoO Electrocatalyst for Superior Hydrogen Evolution." *Journal of Energy Chemistry*, vol. 52, 2021, pp. 33-40. https://doi.org/10.1016/j.jechem.2020.04.036.
14. Hu, Z., et al. "Exploring the Formation of CoO/ZnO Heterostructure to Enhance Electrocatalytic Oxygen Evolution Reaction." *Advanced Materials Interfaces*, vol. 10, no. 16, 2023. https://doi.org/10.1002/admi.202300091.
15. Huang, X., et al. "Enhancing the Electrocatalytic Activity of CoO for the Oxidation of 5-Hydroxymethylfurfural by Introducing Oxygen Vacancies." *Green Chemistry*, vol. 22, no. 3, 2020, pp. 843-849. https://doi.org/10.1039/c9gc03698a.
16. Liang, Z., et al. "Quasi-Single-Crystalline CoO Hexagrams with Abundant Defects for Highly Efficient Electrocatalytic Water Oxidation." *Chemical Science*, vol. 9, no. 34, 2018, pp. 6961-6968. https://doi.org/10.1039/c8sc02294a.
17. Liu, X., et al. "Co Nanoparticles Embedded in a 3D CoO Matrix for Electrocatalytic Hydrogen Evolution." *RSC Advances*, vol. 6, no. 45, 2016, pp. 38515-38520. https://doi.org/10.1039/c6ra07538j.
18. Qi, J., et al. "Aligned Cobalt-Based Co@CoOx Nanostructures for Efficient Electrocatalytic Water Oxidation." *Chemical Communications*, vol. 53, no. 66, 2017, pp. 9277-9280. https://doi.org/10.1039/c7cc04609j.
19. Wang, C., et al. "Active Co@CoO Core/Shell Nanowire Arrays as Efficient Electrocatalysts for Hydrogen Evolution Reaction." *Chemical Engineering Journal*, vol. 429, 2022. https://doi.org/10.1016/j.cej.2021.132226.
20. Zhang, H., et al. "Interfacial FeOOH/CoO Nanowires Array Improves Electrocatalytic Water Splitting." *Journal of Solid State Chemistry*, vol. 298, 2021. https://doi.org/10.1016/j.jssc.2021.122156.
21. Li, W., et al. "Interface Engineering of Heterogeneous CeO_2–CoO Nanofibers with Rich Oxygen Vacancies for Enhanced Electrocatalytic Oxygen Evolution Performance." *ACS Applied Materials & Interfaces*, vol. 13, no. 39, 2021, pp. 46998-47009. https://doi.org/10.1021/acsami.1c11101.
22. Ghosh, P., et al. "Plasmonic CoO-Decorated Au Nanorods for Photoelectrocatalytic Water Oxidation." *ACS Applied Nano Materials*, vol. 2, no. 9, 2019, pp. 5795-5803. https://doi.org/10.1021/acsanm.9b01258.
23. Kim, J.-H., et al. "Enhanced Activity Promoted by CeO_x on a CoO_x Electrocatalyst for the Oxygen Evolution Reaction." *ACS Catalysis*, vol. 8, no. 5, 2018, pp. 4257-4265. https://doi.org/10.1021/acscatal.8b00820.
24. Li, W., et al. "Interface Engineering of Heterogeneous CeO_2–CoO Nanofibers with Rich Oxygen Vacancies for Enhanced Electrocatalytic Oxygen Evolution Performance." *ACS Applied Materials & Interfaces*, vol. 13, no. 39, 2021, pp. 46998-47009. https://doi.org/10.1021/acsami.1c11101.
25. Luo, Y., et al. "Fe_3O_4/CoO Interfacial Nanostructure Supported on Carbon Nanotubes as a Highly Efficient Electrocatalyst for Oxygen Evolution Reaction." *ACS Sustainable Chemistry & Engineering*, vol. 8, no. 8, 2020, pp. 3336-3346. https://doi.org/10.1021/acssuschemeng.9b07292.
26. Sun, Z., et al. "Boosting Electrocatalytic Hydrogen-Evolving Activity of Co/CoO Heterostructured Nanosheets via Coupling Photogenerated Carriers with Photothermy." *ACS Sustainable Chemistry & Engineering*, vol. 6, no. 9, 2018, pp. 11206-11210. https://doi.org/10.1021/acssuschemeng.8b02676.
27. Wang, D., et al. "Ce-Doped Co_3O_4 Nanoplates for Photo-Assisted Methanol Electrocatalytic Oxidation." *New Journal of Chemistry*, vol. 48, no. 33, 2024, pp. 14834-14843. https://doi.org/10.1039/d4nj02109f.
28. Du, Y., et al. "Boosting Electrocatalytic Oxygen Evolution: Superhydrophilic/Superaerophobic Hierarchical Nanoneedle/Microflower Arrays of $Ce_xCo_{3-x}O_4$ with Oxygen Vacancies." *ACS Applied Materials & Interfaces*,

https://doi.org/10.59720/24-333

vol. 13, no. 36, 2021, pp. 42843-42851. https://doi.org/10.1021/acsami.1c11662